Bull. Mater. Sci. (2019) 42:61
https://doi.org/10.1007/s12034-019-1738-z

Detoxification of dye contaminated water by Mn^{2+}-doped ZnS nanostructures

BALWINDER KAUR[1,*], SUBHASH CHAND[1], KARAMJIT SINGH[2] and ASHOK KUMAR MALIK[1]
[1]Department of Chemistry, Punjabi University, Patiala, Punjab 147 002, India
[2]Department of Physics, Punjabi University, Patiala, Punjab 147 002, India
*Author for correspondence (balwindertahem1987@gmail.com)

MS received 1 June 2018; accepted 25 July 2018; published online 6 March 2019

Abstract. Chemical co-precipitation route was successfully employed to synthesize polyethylene glycol-coated pure and doped $Zn_{1-x}Mn_xS$ ($0 \leq x \leq 0.1$) nanoparticles. The crystallographic and morphological analyses have been done by X-ray diffraction (XRD) and transmission electron microscopy (TEM), respectively. The formation of cubic crystal structure and quasi-spherical morphology has been revealed by XRD and TEM, respectively. The optical analyses have been done by UV–Vis absorption spectroscopy and energy resolved photoluminescence spectroscopy. Energy dispersive X-ray spectroscopy study has been carried to analyse the elemental composition. The doping concentration dependent photo-catalytic activity was checked to analyse the photo-catalytic potential of $Zn_{1-x}Mn_xS$ nanoparticles under UV irradiation.

Keywords. Chemical co-precipitation; $Zn_{1-x}Mn_xS$ nanoparticles; photo-catalytic activity.

1. Introduction

In the field of semiconductor industry, II–VI chalcogenide semiconductors have attained a milestone due to its size-customized optical properties. Zinc sulphide (ZnS) nanomaterials possess broad band gaps i.e., cubic- and hexagonal-structured ZnS have 3.68 and 3.77 eV band gap, respectively [1]. ZnS nanomaterials are the backbone of various fields such as electronics to analytical streams [2–7]. In other words, 'ZnS is jack of all trades'. Furthermore, on doping with d-block and f-block elements, the optical properties are transformed i.e., band gap and luminescent centres are amplified in electromagnetic spectrum [8]. In addition, the morphology and crystallography are also redesigned. ZnS nanoparticles can be synthesized by various efficient routes like solvothermal [9,10], sol–gel [11], electrospray pyrolysis [12], polymer precursor [13], reverse micellar synthesis [14] and many more. In the present appraisal, $Zn_{1-x}Mn_xS$ ($0 \leq x \leq 0.1$) nanomaterials have been synthesized by varying doping with Mn^{2+} *via* a facile chemical co-precipitation route. Due to industrialization, gradual dumping of organic/inorganic waste materials in the form of textile dye waste, drugs and many more in soil and rivers are enhanced beyond the safety limit, which is a threat to flora and fauna. The worthiness of a research work is its applicability for the well-being of the whole ecosystem. In continuation, water purification is a strong concern for the society. Clean water for drinking purposes is the primary need of a community. The photo-catalytic activity of synthesized nanomaterials to decompose/degrade organic pollutants as a test contaminant in water has been thoroughly studied to explore the potential of synthesized nanomaterials for purification of polluted water. To the best of our knowledge, this is the first manuscript mentioning the photo-catalytic ability of polyethylene glycol (PEG)-coated $Zn_{1-x}Mn_xS$ ($0 \leq x \leq 0.1$) nanostructures for degradation of an organic pollutant methylene blue (MB) dye.

2. Materials and methods

2.1 *Chemicals required*

Zinc acetate dihydrate [$Zn(CH_3COO)_2{\cdot}2H_2O$], PEG-400 [$C_{2n}H_{4n+2}O_{n+1}$], sodium sulphide [$Na_2S{\cdot}xH_2O$], manganese acetate heptahydrate [$Mn(COOH)_2{\cdot}7H_2O$] and MB dye [$C_{16}H_{18}N_3SCl$] were purchased from Merck. All chemicals were analytical reagent grade with ultrahigh purity and used without further purification. Deionized water and ethanol were used for all sample preparations.

2.2 *Synthesis of PEG-coated pure and Mn^{2+}-doped ZnS nanostructures*

To synthesize ZnS nanostructures, 0.1 M zinc acetate dihydrate solution was prepared by dissolving appropriate amount of precursor in 40 ml of deionized water–ethanol matrix (equal volume) mixed with 15 ml of 2.5% PEG capping agent. Then, followed by stirring, 0.1 M of sodium sulphide in 40 ml of deionized water–ethanol matrix was added drop by drop to the above prepared mixture. A precipitate was formed immediately on mixing zinc and sulphide precursors. Finally, the product was dried in a hot air oven at 120°C for 2 h.

A similar method of preparation was used for the synthesis of $Zn_{1-x}Mn_xS$ nanostructures [15,16].

2.3 *Characterization*

Powder X-ray diffraction (XRD) patterns were recorded for the crystallographic analyses of the synthesized nanostructures. The diffraction patterns were recorded in the 2θ range of 20–65° using a Rigaku Miniflex-600 Powder X-ray Diffractometer by keeping scan speed and step size of 4° min^{-1} and 0.02°, respectively. Transmission electron microscopy (TEM) measurements for morphological analysis were carried out by placing a drop of well dispersed ethanolic solution of nanoparticles on a carbon-coated copper grid. The samples were dried at room temperature and analysed on a Hitachi H-7650 Electron Microscope at accelerating voltage of 100 kV. The UV–Vis absorption spectra of synthesized ZnS nanostructures have been recorded in wavelength range of 280–400 nm, using a Labtronics Spectrophotometer. The photoluminescence spectra of the synthesized samples were analysed on a RF-5301PC Spectrofluorometer by placing the ethanolic solution of nanoparticles in a quartz cuvette of 5 mm path length. The energy dispersive X-ray (EDX) studies were carried out on an Oxford INPA Energy Dispersive Spectrophotometer by mounting the sample on a brass stub for elemental composition analyses. The photo-catalytic activity potential of the synthesized nanostructures was checked under UV light irradiation using MB dye as a test contaminant in aqueous media. The stock solution of the dye was prepared by dissolving 3 mg MB dye in 500 ml of water. Before illumination, the suspension of ZnS nanostructures (0.014 g ZnS in 100 ml dye solution) in the dye, was stirred in the dark for 60 min to equilibrate the solution. After equilibration of solution, the suspension was illuminated in an indigenous UV reactor for 90 min. During irradiation, the aliquots were collected after regular time intervals (15 min) to analyse the photo-degradation of MB dye by UV–Vis absorption spectrophotometer in the visible region (450–700 nm) of electromagnetic spectrum.

3. Results and discussion

3.1 *Crystallographic analyses*

XRD is an important tool to carry out crystallographic analysis. Figure 1a and b shows powder XRD patterns of PEG-coated pure and Mn^{2+}-doped ZnS nanostructures. A comparison of recorded diffraction patterns with standard JCPDS file no. 05-0566 confirms the formation of cubic (zinc blende) structured ZnS nanocrystallites. It is clearly seen in figure 1a that the peaks situated at 2θ values 28.7966, 47.8897 and 56.6946° observed in the case of PEG-coated pure ZnS nanocrystals correspond to crystallographic planes (111), (220) and (311), respectively. On the other hand, it can be clearly seen from recorded diffraction patterns of Mn-doped ZnS nanocrystals (figure 1b) that a slight shifting in peak positions at 2θ values: 28.7715, 47.7630 and 56.4268°, corresponds to similar crystal planes. No diffraction peaks other than ZnS nanocrystals were noted, indicating high purity of the synthesized products. The shifting of XRD lines with doping simply suggest that Mn^{2+} was successfully substituted into the ZnS host structure at the Zn^{2+} site. Furthermore, the ionic radius of Mn^{2+} is 0.80 Å as compared to Zn^{2+}, whose ionic radius is 0.74 Å. Due to a slightly larger ionic radius of Mn^{2+} a lattice strain is built in the ZnS host matrix. Pure ZnS nanocrystals possess high crystalline texture as compared to Mn^{2+}-doped ZnS nanocrystals. The average crystallite size was calculated by Scherrer formula as given below:

$$D = \frac{0.89\lambda}{\beta \cos\theta}$$

where 0.89 is the constant value for shape factor, λ is the X-ray wavelength of Cu radiation, θ is the Bragg diffraction angle and β is the full-width at half-maximum of the highest diffraction peak. The average crystallite size values calculated using the Scherrer formula from recorded diffraction pattern of PEG-coated pure and Mn^{2+}-doped ZnS nanostructures are 4.28 and 3.93 nm, respectively. Figure 2b shows the broadening of diffraction peaks, which reveals the small nanocrystallite size. The strain can be calculated from the Williamson–Hall (W–H) method according to the following equation:

$$\beta \cos\theta = \lambda K/D + 4\varepsilon \sin\theta$$

where $K \sim 1$ is the crystallite shape constant, β is the full-width at half-maximum, D is the average crystallite size and ε is the strain.

The strain is −0.1181 and 0.00364 for PEG-coated pure and Mn^{2+}-doped ZnS nanocrystals, respectively. The lattice parameters of cubic structure were calculated according to the following formula:

$$1/d_{hkl}^2 = h^2 + k^2 + l^2/a^2$$

where a is the lattice parameter and d_{hkl} is the interplanar separation corresponding to *hkl*. The calculated average values of lattice parameter for PEG-coated pure and Mn^{2+}-doped ZnS are 5.3654 and 5.3704 Å (similar to standard JCPDS file no. 05-0566), respectively. The doping of Mn^{2+} in ZnS nanocrystals is further confirmed by EDX spectroscopy as well as optical analyses.

3.2 *EDX spectroscopic analyses*

EDX spectroscopy is a useful analysis tool to check the presence of constituent elements in the synthesized material. Figure 3a and b shows the recorded EDX spectra, which reveal the formation of ZnS by confirming the presence of Zn

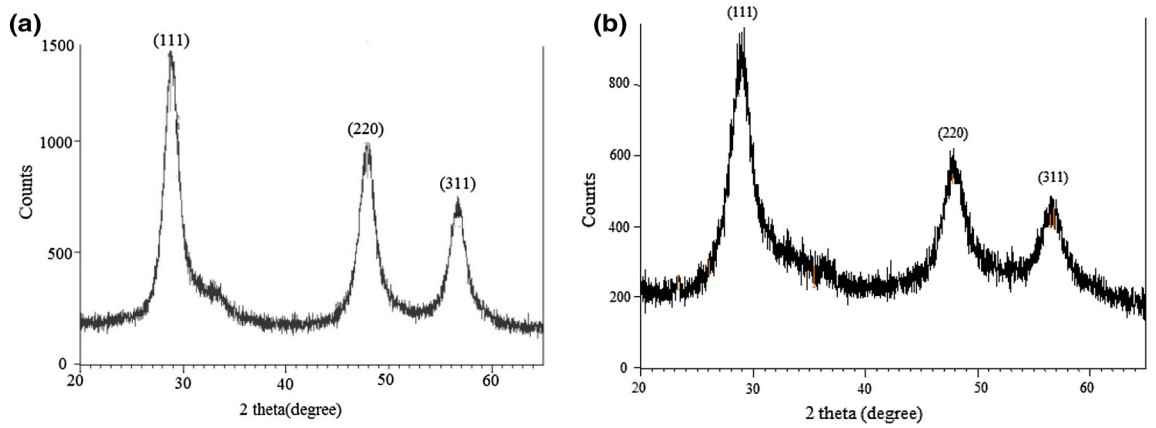

Figure 1. XRD pattern: (**a**) PEG-coated pure ZnS nanocrystals and (**b**) PEG-coated 10% Mn^{2+}-doped ZnS nanocrystals.

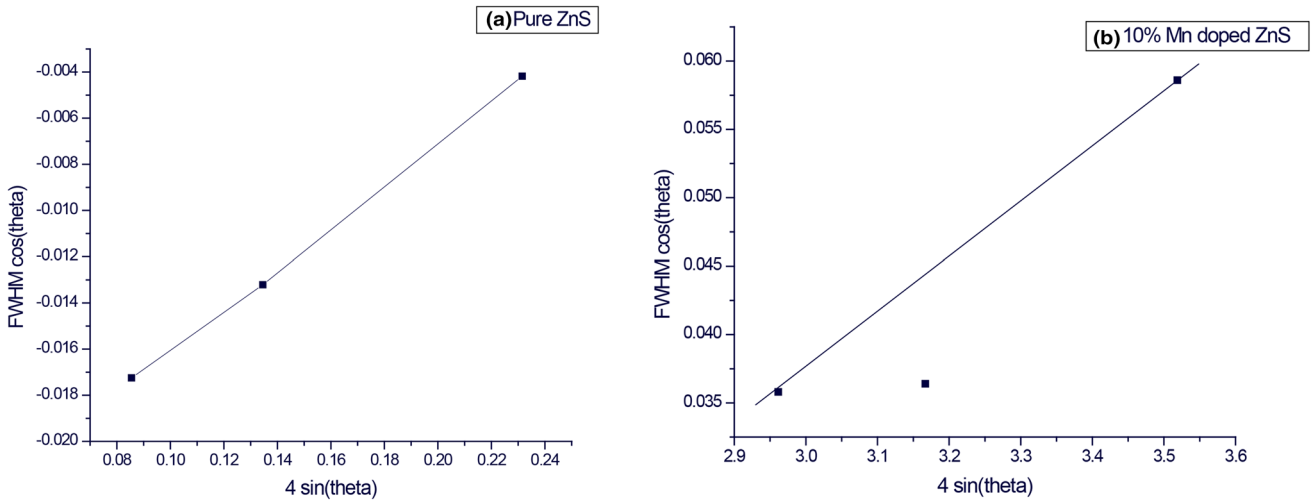

Figure 2. W–H plot for strain: (**a**) PEG-coated pure and (**b**) PEG-coated 10% Mn^{2+}-doped ZnS nanocrystals.

and S elements with weight percentage (atomic percentage) of 59.62 (36.39) and 29.48% (36.59%), respectively. Along with Zn and S, the presence of the other constituent element O has been confirmed and its corresponding weight percentage (atomic percentage) is 10.90% (27.11%).

Similarly, the presence of Zn, S, Mn, O and C elements in Mn^{2+}-doped ZnS have been confirmed and checked by their weight percentage (atomic percentage) as 46.17 (20.49), 23.60 (21.36), 2.42 (1.28), 17.11 (31.03) and 10.70% (25.85%), respectively. The presence of O and C elements is due to atmospheric oxygen and carbon tape, respectively.

3.3 *Morphological analyses*

TEM is an important tool for morphological analysis. The recorded TEM micrographs (figure 4a and b) of PEG-coated pure and Mn^{2+}-doped ZnS nanostructures reveal the formation of quasi-spherical morphology. It can be clearly seen from the recorded micrographs that the synthesized nanostructures have high surface energy, with the presence of a small amount of capping agent layer in synthesized pure ZnS nanoparticles as compared to $Zn_{1-x}Mn_xS$ nanoparticles. The particle size values vary between 4–10 nm and 2–5 nm for PEG-coated pure and Mn^{2+}-doped ZnS nanostructures, respectively. A comparison of XRD and TEM results indicate that the synthesized nanoparticles are single nanocrystals as the average crystallite size values calculated from the recorded diffraction patterns are almost close to the particle sizes measured from electron micrographs.

3.4 *Optical analyses*

UV–Vis absorption spectroscopy is a useful technique to monitor the optical properties of nanomaterials. Recorded UV–Vis absorption spectra of PEG-coated pure and Mn^{2+}-doped ZnS nanostructures are shown in figure 5. The absorption edge is ∼340 nm which is almost similar to bulk material absorption

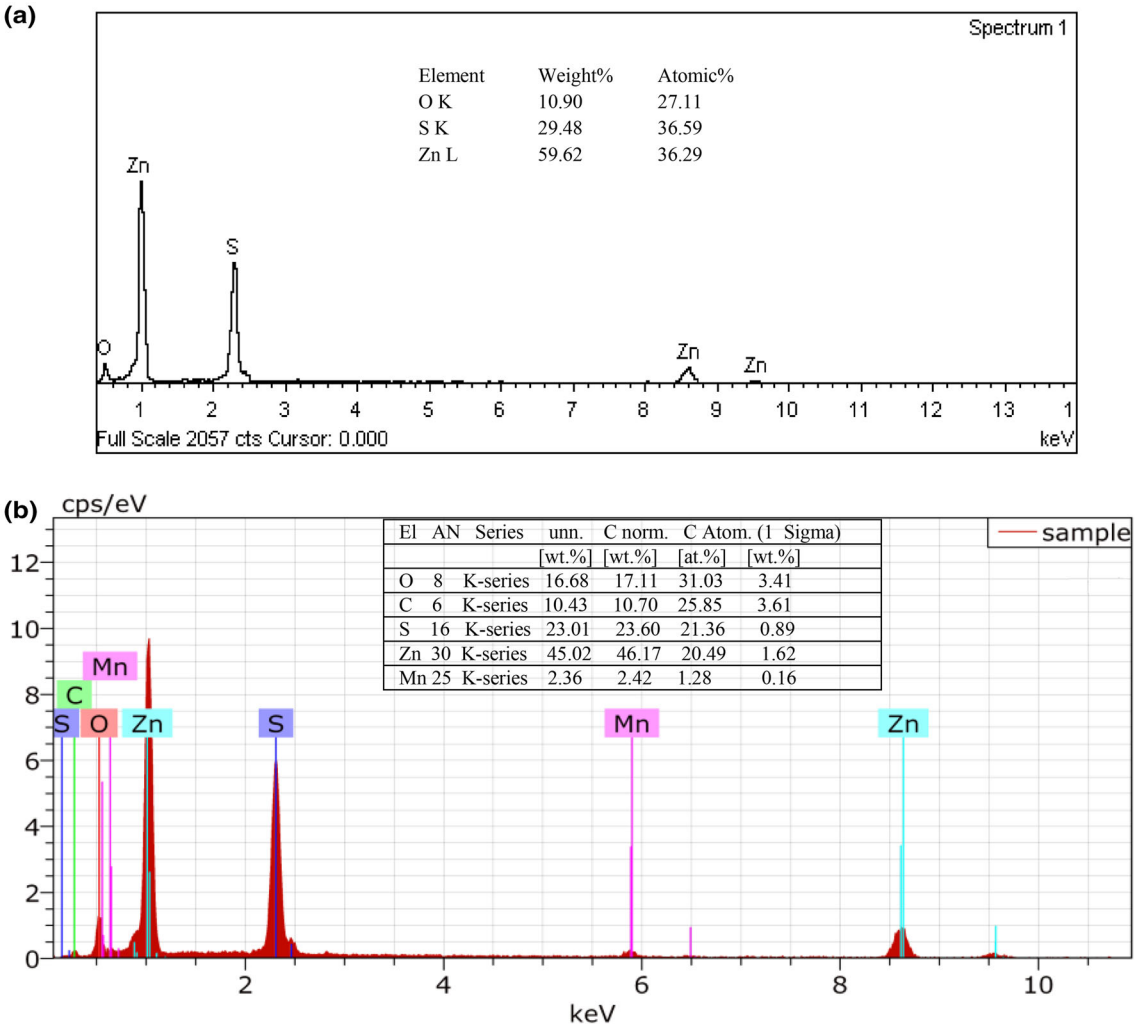

Figure 3. EDX spectra: (**a**) PEG-coated pure and (**b**) PEG-coated 10% Mn^{2+}-doped ZnS nanostructures.

edge, whose band gap is 3.68 eV. PEG-coated pure and Mn^{2+}-doped ZnS nanostructures show a broad absorption profile in the UV region due to broad size distribution of nanostructures which is also confirmed by TEM analysis. The broad absorption profile in the UV region shows that the synthesized materials can be used as a UV photo-catalyst. 10% Mn^{2+}-doped ZnS nanostructures have maximum absorption intensity as compared to pure ZnS nanostructures which have minimal absorption intensity. Hence it is concluded that on increasing the concentration of Mn^{2+} ions in the ZnS host matrix, there is a gradual rise in absorption intensity i.e., a hyperchromic shift is observed.

3.5 *Photoluminescence (PL) studies*

PL provides valuable information about the optical behaviour especially luminescent centres in nanomaterials. The room temperature PL spectra of PEG-coated pure and Mn^{2+}-doped ZnS nanostructures were recorded by excitation at 335 and 290 nm, respectively. Figure 6a illustrates the emission spectra of PEG-coated pure ZnS nanostructures having emission peaks at 410, 433 and 465 nm. The emission at 410 and 433 nm corresponds to interstitial sulphur (I_S) lattice defect and interstitial zinc (I_{Zn}) lattice defect. A weak shoulder at 465 nm is assigned to dangling sulphur bonds at interface of ZnS grains [17]. On substitution of cations of host matrix with Mn^{2+} ions, the amalgamation between the s–p electrons of the host material with 3d electrons of Mn^{2+} and makes the Laporte forbidden transition of $^4T_1 \rightarrow {}^6A_1$ partially allowed, resulting in the orange emission of Mn^{2+} along with UV emission [18]. The weak shoulder at 416 and 418 nm is again due to interstitial sulphur in PEG-coated Mn^{2+}-doped ZnS nanostructures. A very weak band at 454 and 464 nm arise due to sulphur vacancies. If Mn^{2+} ions are adsorbed on the ZnS surface rather than substitution then ZnS nanoparticles result in ultraviolet emission only. Hence, in the present case, it is confirmed that Mn^{2+} is being substituted in the host lattice. The substitution

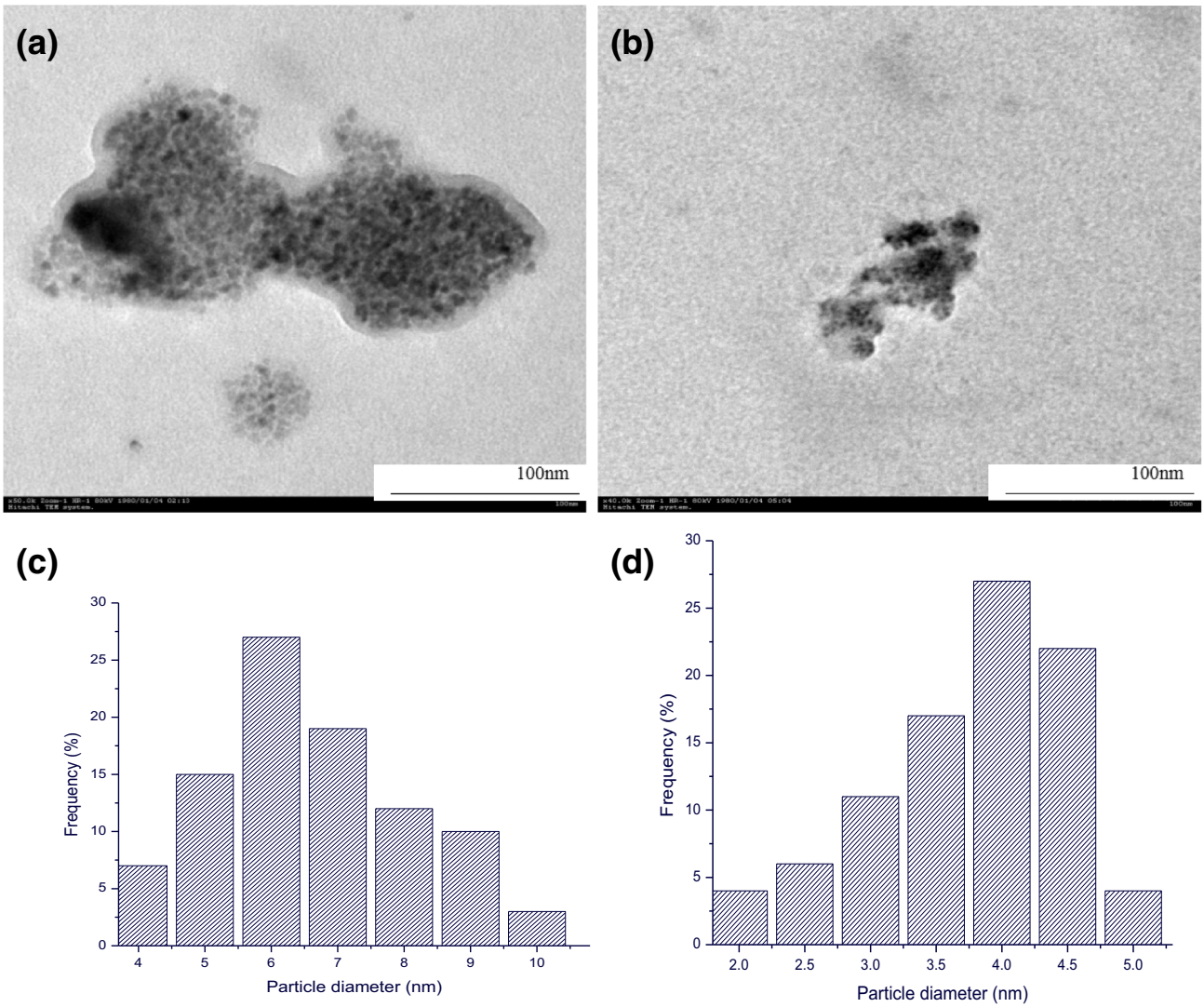

Figure 4. TEM micrographs: (**a**) PEG-coated pure; (**b**) PEG-coated 10% Mn^{2+}-doped; (**c**) histogram of PEG-coated pure and (**d**) histogram of PEG-coated 10% Mn^{2+}-doped ZnS nanostructures.

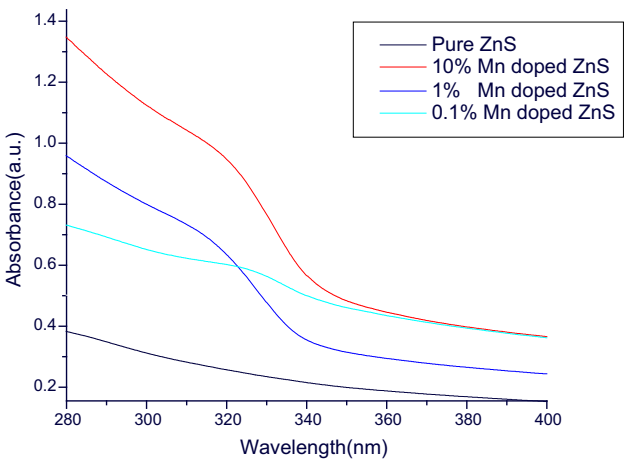

Figure 5. UV–Vis absorption spectra of PEG-coated pure and Mn^{2+}-doped ZnS nanostructures.

of Mn^{2+} ion in the host matrix is also confirmed by EDX analysis. The characteristic orange emission occurs at ~590 nm as observed by various research groups. Similarly, orange emission is observed in figure 6b–d with a slight shift in the wavelength position. Such a broad asymmetric emission at 590 nm originates with Mn^{2+} ion if it is present at tetrahedral lattice, whereas a sharp emission at 603 nm arises due to the presence of Mn^{2+} ions in octahedral interstitials. Goedet *et al* [19] have observed emission peaks of α-MnS films at around 680 nm due to $^6A_1(6S) \rightarrow {}^4T_2(4G)$ transition. α-MnS crystals come into existence only if the Mn^{2+} concentration exceeds the optimum concentration limit. Such emission is not observed in present investigation. The characteristic emission (orange emission) peaks due to Mn^{2+} keeps increasing with the increase in doping content. Furthermore, doping Mn^{2+} ions in ZnS host matrix enhances the life time of e^- and h^+ i.e., excited charge carrier. This is known as interfacial charge transfer

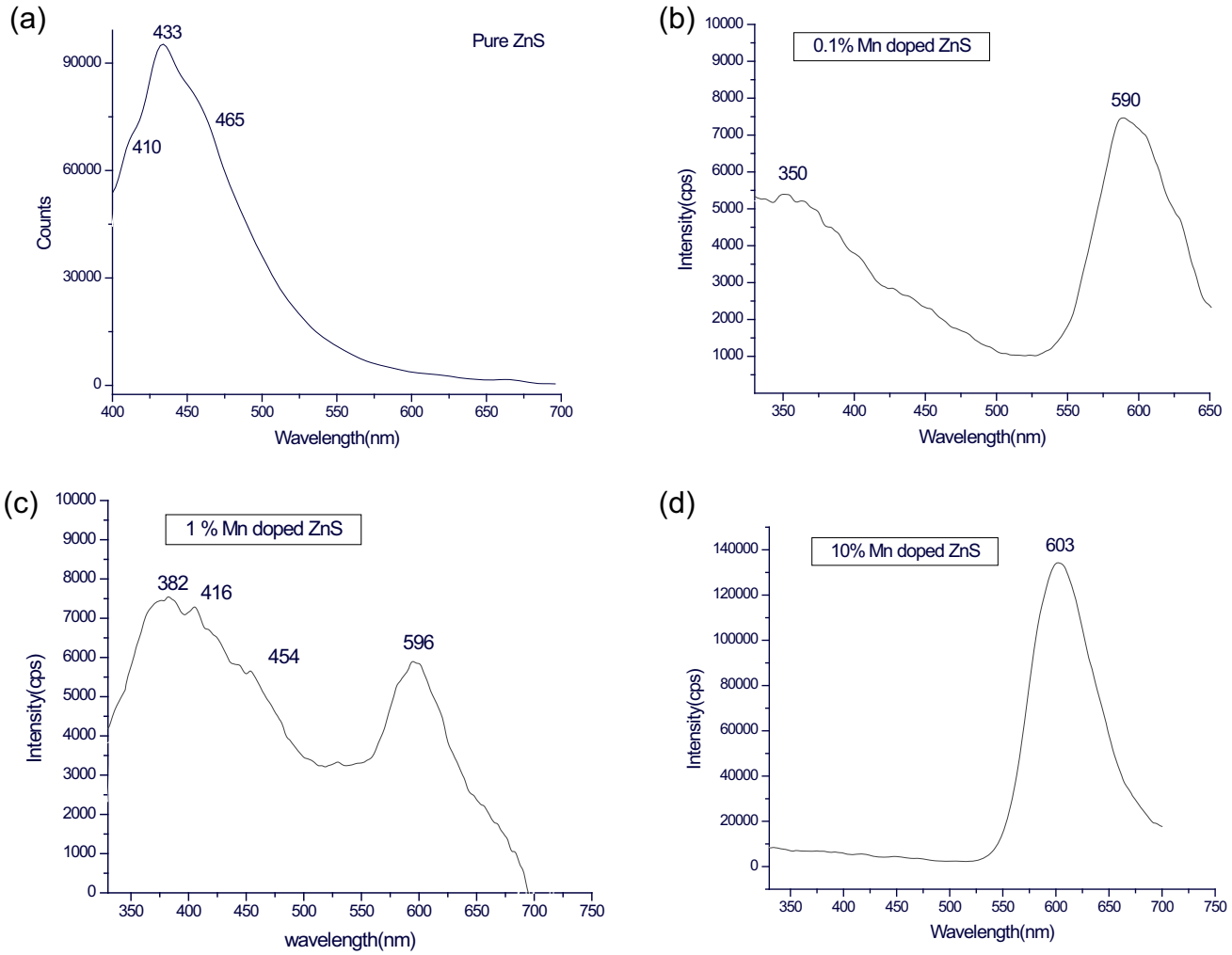

Figure 6. PL spectra of synthesized nanostructures: (**a**) PEG-coated pure; (**b**) PEG-coated 0.1% Mn^{2+}-doped; (**c**) PEG-coated 1% Mn^{2+}-doped and (**d**) PEG-coated 10% Mn^{2+}-doped ZnS nanostructures.

and this probably increases the photo-catalytic potential of the synthesized materials. On the other hand, recombination of trapped carriers leads to PL, which decreases the photo-catalytic activity.

3.6 *Photo-catalytic degradation of dye solution*

The photo-catalytic degradation of MB dye in aqueous media by synthesized ZnS nanostructures was carried out under UV irradiation. When a UV photon ($h\nu$) interacts with ZnS nanostructures dispersed in MB dye contaminated aqueous solution, electrons (e^-) from the valence band move to the conduction band, leaving behind a hole (h^+) in the valence band. Actually, the synthesized $Zn_{1-x}Mn_xS$ nanostructures are efficient photo-catalysts in the UV region rather than visible light. Since the band gap of synthesized materials lie in the UV region, UV radiation is appropriate for the generation of e^- and h^+ pair. There are two major possibilities: either photo-generated e^- and h^+ can recombine through radiative/non-radiative processes to undergo a vibrational cascade-like process or these can be trapped in defect states created by impurity followed by recombination or transferred to the nanostructure surface to undergo surface reactions like photo-catalytic activity, where these may interact with species adsorbed (covalently bonded) on or close to the surface (physically adsorbed) of the nanostructure. Here, the valence band holes react with the chemisorbed (covalently absorbed) H_2O molecules to form reactive free radicals such as $OH^\bullet$, whereas conduction band electrons interact with dissolved O_2 to form $OH^\bullet$ radicals, which subsequently react with dye molecules to cause their complete degradation. Photo-catalytic efficiency of ZnS nanostructures mainly depends upon amount of $OH^\bullet$ radicals generated. Therefore, any factor that supports the generation of $OH^\bullet$ radicals will enhance the rate of photo-catalytic degradation of MB dye [20]. The mechanism of the photo-catalytic reaction can be

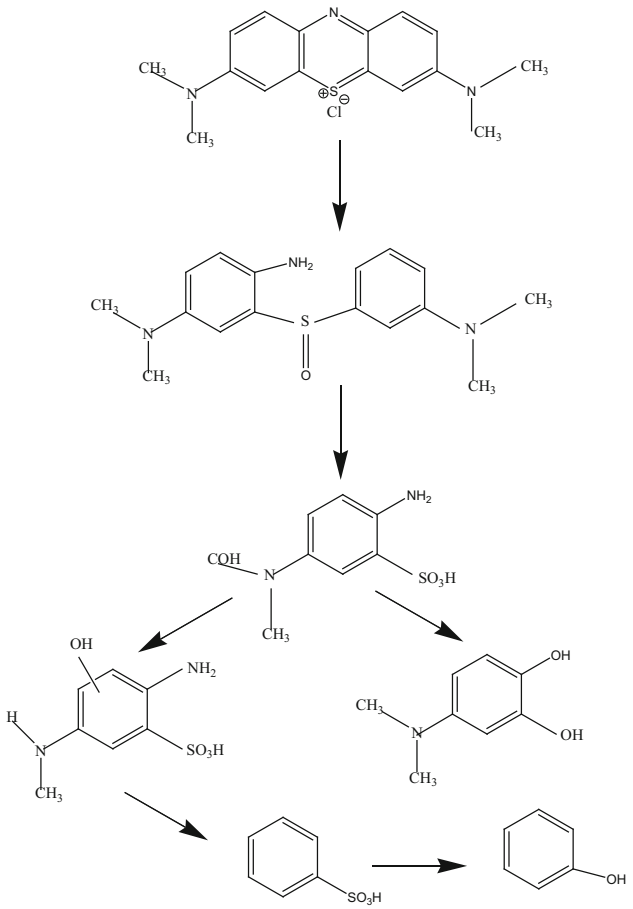

Figure 7. Degradation pathways of MB dye.

described as follows:

$$ZnS + h\nu\ (UV) \rightarrow ZnS^{\bullet}(h^{+} + e^{-})$$

The oxidation of water by holes $[H_2O \leftrightarrow H^{+} + OH^{-}]$

$$h^{+} + H_2O \rightarrow OH^{\bullet}$$

$$O_2 + e^{-} \rightarrow O_2^{\bullet}$$

$$2H_2O + e^{-} + O_2^{\bullet} \rightarrow 2OH^{\bullet} + 2OH^{-}$$

$$OH^{\bullet}/O_2^{-\bullet} + C_{16}H_{18}N_3SCl \rightarrow CO_2 + H_2O + SO_4^{2-} + NH_4^{+}Cl^{-}.$$

The conversion of MB dye into simpler molecules like CO_2, SO_4^{2-}, NH_4^{+}, etc. occurs after heterocyclic and homocyclic ring cleavages as shown in figure 7. After ring cleavages of MB dye, the complete mineralization of MB dye is done *via* various reactive intermediates like $OH\cdot/O_2^{-\bullet}$ to easily remove the nontoxic gases and ions. The schematic photo-catalytic degradation pathways of MB dye by reactive free radicals has been described in figure 7 [17,21]. Ahmad *et al* [22] reported the mass spectrum of fully degraded MB dye. The dye concentration as the function of UV irradiation time was analysed using a UV–Vis absorption spectrophotometer.

The degradation % of dye could be calculated using the following formula:

$$C\ (\%) = [(A_0 - A)/A_0] \times 100$$

where C is the degradation percentage, A_0 and A are the absorption of dye solution before and after photo-catalysis, respectively. Figure 8 shows the absorbance profile of MB dye with respect to wavelength, degraded by $Zn_{1-x}Mn_xS$ ($0 \leq x \leq 0.1$) nanoparticles. The photo-catalytic efficiency basically depends upon the generation of photo-excited carriers followed by their surface transfer dominance over the radiative recombination. The photo-catalytic activity is a phenomenon which takes place by absorption of photons from suitable source of light. The absorbance of synthesized nanomaterials in UV radiation lies in the order: 10% Mn^{2+}-doped ZnS > 1% Mn^{2+}-doped ZnS > 0.1% Mn^{2+}-doped ZnS > pure ZnS. It is obvious that the greater the absorption of photons greater will be the generation of reactive free radicals. A similar trend is observed with photo-catalytic behaviour of synthesized materials. The greater the absorption of photons by the catalyst, higher will be its potential to degrade the adsorbed pollutants or lesser will be the residual dye % in aliquots. Furthermore, photo-catalytic activity is favourable with participation of e^{-} and h^{+} pairs (charge carriers) with surface phenomena (photoredox chemistry) rather than radiative recombination with bulk atoms. In short, there are two primary phenomenon associated with photo-catalytic activity: absorption of photons followed by participation in surface reactions. Also, the lesser the area of cross-section in PL study, greater would be the participation of e^{-} and h^{+} pairs (charge carriers) with surface reactions such as photo-catalytic activity as in present research work. In other words, the higher the number of charge carriers on surface or lengthening of excited state life time of charge carriers, much lesser are the chances of radiative/non-radiative recombination (vibrational cascade, fluorescence, etc.) associated to e^{-} and h^{+} pairs i.e., there is competition between charge carrier recombination with charge carrier trapping. Hence, the higher the interfacial charge transfer/charge carrier trapping the higher would be the photo-catalytic activity. The residual dye % is higher in the case of pure ZnS nanoparticles, whereas residual dye % is less in Mn^{2+}-doped ZnS nano-photo-catalysts. Furthermore, $Zn_{0.90}Mn_{0.1}S$ and $Zn_{0.99}Mn_{0.01}S$ nano-photo-catalysts degrade 94.80 and 90.20% dye in 90 min, respectively. Also, degraded dye % is 88.20 by $Zn_{0.999}Mn_{0.001}S$ nano-photo-catalysts, respectively as compared to pure ZnS nanoparticles, which degrades 80% dye. Mn-doped ZnS nanoparticles are efficient photo-catalysts as compared to pure ZnS nanoparticles. Hence, more the absorption of UV light greater will be the discoloration ability. Pristine dye solution was also irradiated for 90 min in a UV reactor to check the photo-bleaching of MB dye, but no photo-bleaching of MB dye was observed. Hence, the synthesized nanostructures are efficient photo-catalysts to degrade the MB dye. Figure 9 shows degradation profile of MB dye with respect to time by $Zn_{1-x}Mn_xS$ ($0 \leq x \leq 0.1$) nano-photo-catalysts.

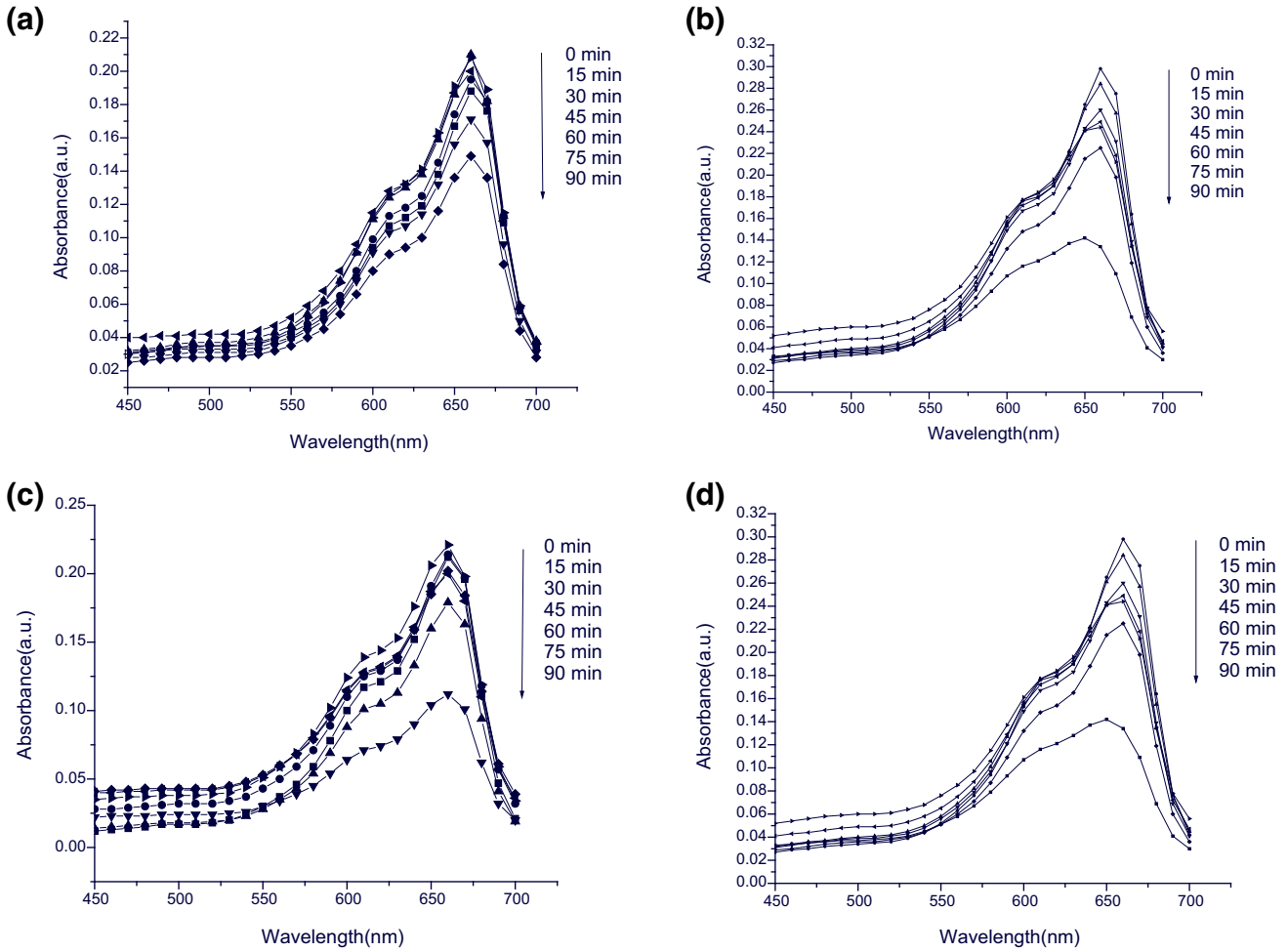

Figure 8. Degradation profile of MB dye: (**a**) by PEG-coated pure; (**b**) by PEG-coated 0.1% Mn^{2+}-doped; (**c**) by PEG-coated 1% Mn^{2+}-doped and (**d**) by PEG-coated 10% Mn^{2+}-doped ZnS nanostructures.

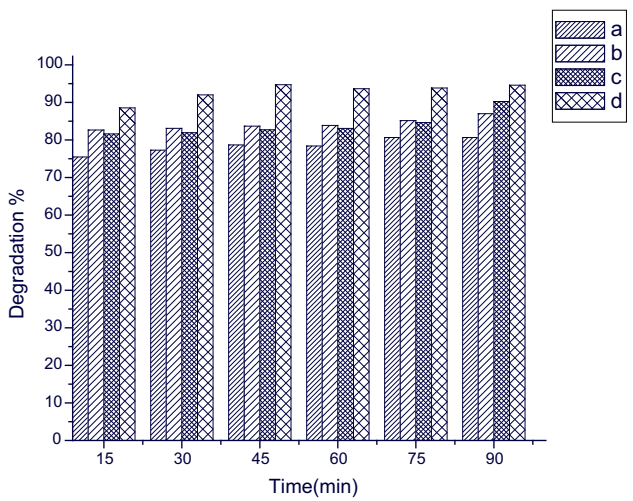

Figure 9. Degraded dye % *vs.* time: (**a**) PEG-coated pure; (**b**) PEG-coated 0.1% Mn^{2+}-doped; (**c**) PEG-coated 1% Mn^{2+}-doped and (**d**) PEG-coated 10% Mn^{2+}-doped ZnS nanostructures.

4. Conclusions

The chemical co-precipitation route of synthesis is an eco-friendly method which yields highly pure nanoparticles. Cost effectiveness and less time consumption are the two major merits of the selected route of synthesis. Cubic phase with well crystalline textures, along with average crystallite size values ~4.28 and 3.93 nm for pure and Mn^{2+}-doped ZnS nanostructures, are observed from XRD studies. The successful incorporation of impurity (Mn^{2+} ion) in the ZnS lattice was examined by EDX spectroscopy. TEM micrographs depict quasi-spherical morphology with particle size range 4–10 nm and 2–5 nm for pure and Mn^{2+}-doped ZnS nanostructures, respectively. Optical analyses tools like UV–Vis spectroscopy and PL study have concluded about the absorption profiles and luminescent centres, respectively in synthesized nanoparticles. The synthesized nanoparticles exhibit a broad absorption profile in UV region of electromagnetic spectrum, which makes these materials reliable for photocatalytic activity in UV region of electromagnetic spectrum.

Multichromatic emission in both UV and visible regions are observed by PL study. Hence, broad absorption profiles and small radiative recombination cross-sections make these materials suitable for photo-catalytic applications. As synthesized $Zn_{0.90}Mn_{0.01}S$ nanoparticles degrade up to 94.80% of dye in water. Hence, Mn^{2+}-doped ZnS nanoparticles are proven to be efficient nano-photo-catalysts.

Acknowledgements

One of the authors, Mrs Balwinder Kaur is thankful to University Grants Commission (UGC), New Delhi, India for providing financial support under scheme Maulana Azad National Fellowships (MANF). The author is obliged to Sophisticated Instrument Centre, Punjabi University, Patiala for providing necessary facilities. The author is grateful to EMN laboratory Punjab Agriculture University, Ludhiana for TEM analysis.

References

[1] Biswas S and Kar S 2008 *Nanotechnology* **19** 045710
[2] Matsui I 2005 *J. Chem. Eng. Jpn.* **38** 535
[3] Huang C Y, Wang D Y, Wang C H, Chen Y T *et al* 2010 *ACS Nano* **10** 5849
[4] Ayodhya D and Veerabhadram G 2016 *J. Fluoresc.* **26** 2165
[5] He Y, Wang H F and Yan X P 2008 *Anal. Chem.* **80** 3832
[6] Sung T W and Lo Y L 2012 *Sens. Actuators B: Chem.* **165** 119
[7] Koneswaran M and Narayanaswamy R 2009 *Sens. Actuators B: Chem.* **139** 104
[8] Hu H and Zhang W 2006 *Opt. Mater.* **28** 536
[9] Hu Z, Li L, Zhou X, Fu X and Gu G 2006 *J. Colloid Interface Sci.* **294** 328
[10] Ahmad T, Khatoon S, Coolahan K and Lofland S E 2013 *J. Mater. Res.* **28** 1245
[11] Planelles-Arago J, Julian-Lopez B, Cordoncillo E, Escribano P, Pellé F, Viana B *et al* 2008 *J. Mater. Chem.* **185** 193
[12] Lenggoro I W, Okuyama K, de la Mora J F and Tohge N 2000 *J. Aerosol Sci.* **31** 121
[13] Al-Hartomy O A, Ubaidullah M, Kumar D, Madani J H and Ahmad T 2013 *J. Mater. Res.* **28** 1070
[14] Ahmad T, Ramanujachary K V, Lofland S E and Ganguli A K 2006 *J. Chem. Sci.* **118** 513
[15] Cholan S, Shanmugam N, Kannadasan N, Sathish Kumar K and Deivam K 2014 *J. Mater. Res. Technol.* **3** 222
[16] Viswanath R, Naik H B, Kumar G Y, Kumar P P, Harish K N, Prabhakara M C *et al* 2014 *Appl. Surf. Sci.* **301** 126
[17] Kaur B, Singh K and Malik A K 2017 *Dyes Pigments* **142** 153
[18] Bhargava R N, Gallagher D, Hong X and Nurmikko A 1994 *Phys. Rev. Lett.* **72** 416
[19] Goede O, Heimbrodt W and Weinhold V 1986 *Phys. Status Solidi b* **136** K49
[20] Viswanath R, Naik H B, Kumar G Y, Kumar P P, Kumar G A and Praveen R 2014 *J. Lumin.* **153** 446
[21] Houas A, Lachheb H, Ksibi M, Elaloui E, Guillard C and Herrmann J M 2001 *Appl. Catal. B* **31** 145
[22] Ahmad T, Phul R, Alam P, Lone I H, Shahazad M, Ahmed J *et al* 2017 *RSC Adv.* **7** 27549